CME DISTURBANCE FORECASTING

G. SISCOE[1,*] and R. SCHWENN[2]
[1]*Center for Space Physics, Boston University, Boston, MA, USA*
[2]*Max-Planck-Institut für Sonnensystemforschung, Katlenburg-Lindau, Germany*
*(*Author for correspondence: E-mail: siscoe@bu.edu)*

(Received 27 June 2006; Accepted in final form 10 July 2006)

Abstract. CME disturbances at Earth arise from the sheath that arrives in front of the ICME and from the ICME itself. The geoeffective environment is qualitatively different in the sheath than within the ICME. Consequently two types of forecast procedures using solar observations of phenomena associated with the release of the CME as input parameters have been developed to treat the two types of environment. This chapter surveys efforts that have resulted in implementable (at least in principle) forecast algorithms for sheath and ICME disturbances and discusses uncertainties associated with both.

Keywords: space weather, storm forecasting

1. Background

CMEs are the hurricanes of space weather – the storms with the greatest potential to inflict damage (e.g., Echer *et al*., 2006). As with all storms, whether in the atmosphere or in space, the forecaster is interested in when it will start and how intense it will be.

For recent reviews of aspects of space weather that pertain to the solar and heliospheric environments, the reader might consult Joselyn (1995), Crooker (2000) and Schwenn (2006). The symptoms of space weather (including CME disturbances) as manifested through its effects on technological systems and human activities have been well described, for example, by Oldenwald (2001), Freeman (2001), and Carlowicz and Lopez (2002). This chapter applies results of CME research described in other chapters of this volume to discuss amelioration of space-weather symptoms as far as is currently possible through predicting the beginning and intensity of CME disturbances.

CME storms manifest separate magnetic and energetic particle phases. Both affect terrestrial systems, while the latter also affect spacecraft and human activities beyond the magnetosphere. The discussion here will be restricted to magnetic disturbances. These have longer lead times and, so, have greater potential for amelioration through forecast algorithms.

Space Science Reviews (2006) 123: 453–470
DOI: 10.1007/s11214-006-9024-y

2. Arrival Times of CME Disturbances

Forecasting the onset of CME disturbances from solar or coronal signatures could give one-to-four day advance warnings. The forecaster is concerned with the arrival of both the ICME shock and the ICME itself, since shocks can arrive with no following ICME ejecta (an off-center impact) and vice versa (a 'slow' ICME, subsonic with respect to the solar wind flow). Models to forecast the arrival time of ICME disturbances divide into empirical and physics-based.

2.1. Empirical Models of CME-Disturbance Arrival Time

Empirical models consist mostly of algebraic algorithms obtained by fitting curves to scatter plots of measured disturbance arrival times versus some measure of speed of a halo CME (see discussion in Section 3.2 of Forsyth *et al.*, 2006, this volume). Schwenn *et al.* (2001, 2005) define the CME "expansion speed" ($V_{\rm exp}$) as the speed at which the CME expands in a direction perpendicular to its direction of propagation. As Figure 1A shows, this definition has the advantage that, unlike the apparent CME speed in the plane of the sky ($V_{\rm PS}$), $V_{\rm exp}$ is independent of the direction of motion of the CME relative to the viewer's line of sight. Regarding the relation between $V_{\rm exp}$ and the actual radial speed of the front of the CME moving

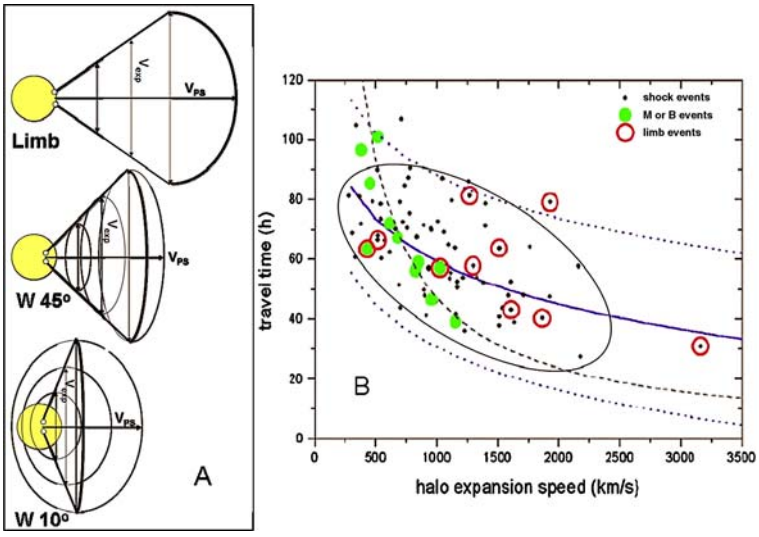

Figure 1. A. Sketch to illustrate the definition of expansion velocity $V_{\rm exp}$ and plane-of-sky velocity $V_{\rm PS}$ (after Schwenn *et al.*, 2005). B. Scatter plot of shock travel times and associated halo expansion speeds. Solid curve gives optimal fit to the functional form $y = a + b\ln(x)$. Dotted lines show two-standard deviation from the optimal fit. Dashed line gives travel time based on constant velocity. (Modified from Schwenn *et al.*, 2005).

away from the Sun ($V_{\rm rad}$), Dal Lago *et al.* (2003) found $V_{\rm rad} = 0.88 V_{\rm exp}$ in an analysis of 57 CME-shock associations within 30° of the limb where $V_{\rm rad}$ could be accurately measured.

Figure 1B shows a scatter plot of 75 CME disturbance travel times versus $V_{\rm exp}$. The dashed line gives the travel time based on the assumption of constant $V_{\rm rad}$ and the Dal Lago *et al.* relation between $V_{\rm exp}$ and $V_{\rm rad}$. (The ellipse enclosing most of the points is a shape-and-position template for use with Figure 2.) When $V_{\rm exp} >$ 800 km/s, most shocks arrive late relative to the constant-speed curve, implying deceleration. Schwenn *et al.* used the kinematics of viscous deceleration in a static medium to arrive at the following expression for the transit time ($T_{\rm SH}$) (though this is not the actual solution of the problem),

$$T_{\rm SH}({\rm h}) = 203 \; - \; 20.77 \; \ln(V_{\rm exp}({\rm km/s})) \tag{1}$$

in which the constants optimally fit the data (solid curve in Figure 1B) (Schwenn *et al.*, 2005). This equation for $T_{\rm SH}$ represents an algorithm that in principle could give one-to-four day operational predictions of the arrival time of ICME shocks. The standard deviation of the scatter around the prediction is 14 h. The dotted lines in Figure 1b mark two standard deviations within which 95% of the points lie.

Gopalswamy *et al.* (2000, 2001) have developed an algorithm for predicting the arrival time of an ICME itself (not of its shock, if it has one) from observations of the ICME's halo-CME phase. The algorithm is based on the kinematics of constant acceleration (or deceleration) between the corona and some distance within 1 AU followed by motion at constant speed. As its initial velocity the algorithm uses the maximum plane-of-sky speed of a halo CME ($V_{\rm PS}$ in Figure 1A). Thus, the algorithm is

$$T_{\rm CME,1} = \frac{-V_{\rm PS} + \sqrt{V_{\rm PS}^2 + 2aD}}{a}; \quad T_{\rm CME,2} = \frac{1 \text{ AU} - D}{\sqrt{V_{\rm PS}^2 + 2aD}} \tag{2}$$

where a and D are the acceleration and the acceleration-cessation distance, and $T_{\rm CME,1}$ and $T_{\rm CME,2}$ are the travel times from the Sun to D and from D to 1 AU, respectively. Obviously, the total travel time is the sum of $T_{\rm CME,1}$ and $T_{\rm CME,2}$. The value $D = 0.76$ AU seems to give best overall results. The acceleration, a, depends on $V_{\rm PS}$, since slow CMEs must accelerate up to solar wind speed and fast CMEs decelerate. Gopalswamy *et al.* (2001) have determined the dependence using concomitant CME observations and in-situ data from spacecraft at quadrature with which to identify the first signature of an arriving ICME (not its shock). They find

$$a({\rm m/s^2}) = 2.193 \; - \; 0.0054 \; V_{\rm PS}({\rm km/s}) \tag{3}$$

Figure 2 compares predictions of the Gopalswamy *et al.* algorithm with 47 halo CME events for which ICME signatures could be identified in Wind or ACE data (Gopalswamy *et al.*, 2001). The 18 h deviation lines contain 88% of the points. The

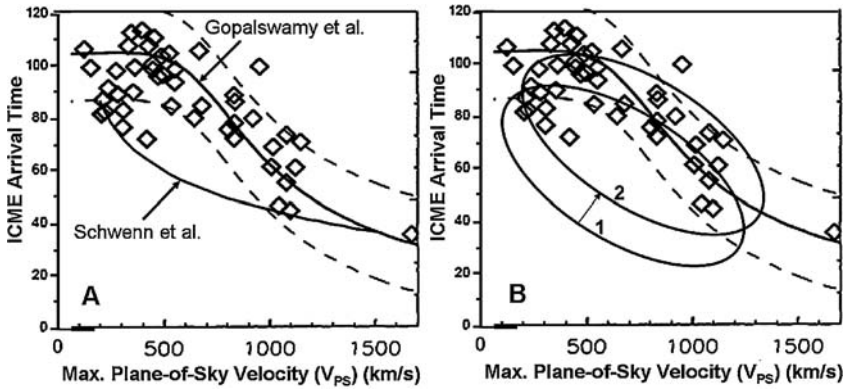

Figure 2. A. Observed ICME arrival times compared with prediction of Equations (2) and (3) (Gopalswamy *et al*. curve). Dashed lines show 18 h deviations from predicted times. The Schwenn *et al*. curve is mapped onto this figure from Figure 1 under the assumption $V_{PS} = V_{exp}/2$. B. Ellipse 1 corresponds to that in Figure 1 under the same mapping assumption. Ellipse 2 is Ellipse 1 shifted vertically to account for an average 12-h lag between shock and ICME arrivals and horizontally to enclose the maximum number of points (100 km/s) (adapted from Gopalswamy *et al*., 2001).

flat part of the curve for $V_{PS} < 500$ km/s suggests that initially slow- and medium-speed CMEs are swept into the solar wind and are merely advected out to 1 AU and, thus, all have a typical 100 h solar wind arrival time.

Figure 2a shows the Schwenn *et al*. curve mapped from Figure 1 assuming that $V_{PS} = V_{exp}/2$, which is appropriate to a strictly circular, Sun-centered halo CME. The Schwenn *et al*. and Gopalswamy *et al*. prediction curves differ considerably for $V_{PS} < 1000$ km/s, but two corrections are to be expected since one curve refers to ICME shocks and the other to ICMEs themselves. First, ICMEs follow their shocks by typically between 6 and 12 hours (with big variations, of course) (Russell and Mulligan, 2002), which means that the Schwenn *et al*. curve should be shifted up to longer times to compare with ICME arrival times, and such a shift brings the curves closer. Second, in general a halo CME is not a circle so that in general $V_{PS} > V_{exp}/2$, and thus the Schwenn *et al*. curve should be shifted to the right to higher speeds to compare with the Gopalswamy V_{PS}-based algorithm. This also brings the curves closer.

Figure 2b carries out the mentioned shifts on the ellipse of Figure 1 (labeled 1). Clearly it poorly overlaps the data points before shifting. Shifting it 12 h up and (a not-unreasonable) 100 km/s to the right gives ellipse 2, which encloses a maximum number of points. The result is somewhat reassuring considering that the two data sets fitted in Figures 1 and 2 are completely different. Moreover, even without shifting, the two curves predict about the same arrival times for high initial speeds ($V_{PS} > 1000$ km/s), when, owing to the high speed, one expects the ICME to arrive shortly after its shock.

A major part of the differences between the two prediction curves results from the formal structure of the fitting algorithms – the Schwenn *et al*. curve has a built-in steep rise for small initial speeds and the Gopalswamy *et al*. curve has a built-in plateau for small initial speeds. Both cases are based on an analog to a simple analytic kinematic model. But even if one were to use more comprehensive analytical dynamical models as discussed in Forbes *et al*. (2006, this volume), little improvement would result. The message of the Schwenn and Gopalswamy fitting efforts is that state-of-the-art empirically-based algorithms predict arrival times of ICME disturbances with uncertainties (at the 90% level) of about plus-or-minus one day.

As was concluded earlier from Helios/Solwind studies, Schwenn *et al*. (2005) maintain that empirical algorithms (specifically, halo CME-based algorithms) are inherently incapable of reducing the stated uncertainty because it arises from variations between the Sun and Earth in the interplanetary medium into which an ICME propagates. By numerically running shock waves through different solar wind conditions, Heinemann (2002) found that that the uncertainty such differences impose on the predicted shock transit time is about plus-or-minus 25% of the predicted transit time (i.e., fast shocks have a smaller absolute arrival-time uncertainty than slow ones). It appears that the Schwenn *et al*. algorithm achieves close to the Heinemann lower limit on forecast uncertainty. Therefore, any hope to reduce the uncertainty further must lie in algorithms that can adjust an ICME's propagation speed in response to predicted variations in the upstream conditions. Such algorithms require physics-based numerical models.

2.2. Physics-Based Models of CME-Disturbance Arrival Time

Three physics-based models are currently being used to predict the arrival times of ICME shocks. They amount to different parameterizations of the physics of a shock wave propagating from a localized region near the Sun into a pre-existing solar wind. In one, the Shock Time of Arrival model (STOA) (Dryer, 1974), a shock wave is assumed to be driven at constant speed (equal to the coronal-density-dependent speed inferred from the event-associated metric type II radio frequency drift rate) for a time set by the duration of the event-associated soft X-ray emission (measured by the GOES satellite) into a Parker-solution solar wind with a speed at 1 AU equal to that measured at L1 at the time of the event. After the driving phase, the shock speed decreases with the $R^{-1/2}$ fall-off (where R is distance from the Sun) appropriate to a blast wave (Parker, 1963). This plus an assumed shock shape determine when the shock will arrive at Earth. The energy that the shock initially acquires during its prescribed launch (speed plus duration) together with the assumed shock shape and the assumed solar wind conditions determine how fast the shock weakens and, so, its strength at Earth.

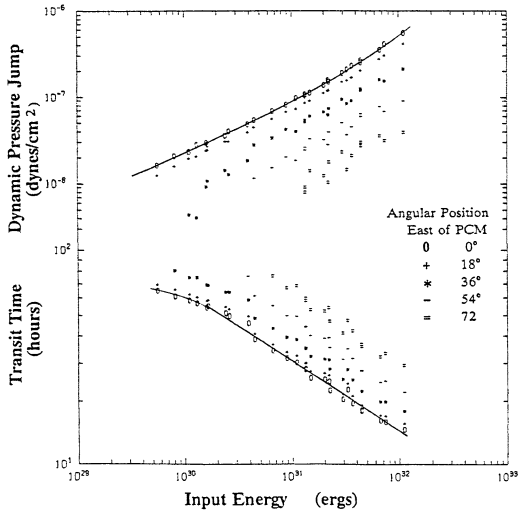

Figure 3. Results of MHD simulations of shocks propagating into a prescribed solar wind (used to parameterize the ISPM) showing how the time of arrival and shock strength at Earth depend on the initiating energy and solar longitude (from Smith and Dryer, 1990).

The second operational physics-based model, the Interplanetary Shock Propagation Model (ISPM) (Smith and Dryer, 1990), consists of analytical fits to results from a numerical MHD shock code (shown in Figure 3) using the same input parameters as STOA. Initial shock energy and location are the only input variables, not solar wind speed (unlike STOA).

The third operational physics-based model, the Hakamada-Akasofu-Fry version 2 model (HAFv2) (Fry *et al.*, 2001), uses the same data inputs as the others to specify the initial shock parameters but differs from them in using the NOAA-produced source-surface velocities near the Sun to generate an inhomogeneous solar wind. At the time of the event, over the event site, source surface velocities are replaced for a certain duration by shock-derived values. A stream-penetration-preventing kinematic algorithm is used to propagate solar wind parcels out from the source surface. The stream-penetration-preventing feature of the algorithm causes fast-moving parcels to bunch up, simulating a shock surface propagating into the inhomogeneous wind. An empirically-calibrated, gradient-threshold criterion is used to identify the shock.

The three physics-based prediction algorithms allow an assessment of the improvement physics-based makes over empirical models and the improvement that incorporating solar wind inhomogeneities makes. Fry *et al.* (2003) applied the STOA, ISPM, and HAFv2 models to 173 events to compile statistics on their performance. All three models show positive skill at the 20% level relative to predictions based on the average shock transit time for the 173 events. The root-mean-square error in predicted shock arrival times was 12.2 h, 11.2 h, and 11.6 h in the order STOA,

ISPM, HAFv2. Thus, perhaps not surprisingly, there is a 2 to 3 hour improvement compared to the 14 h RMS error for the Schwenn *et al*. algorithm. More interesting is the lack of a significant improvement between the HAFv2 model, which incorporates a constantly updated representation of the inhomogeneous solar wind into which the shock propagates, and the ISPM (with no solar wind adjustment) and STOA (with only a one-time, single speed adjustment) models. Either the kinematical treatment of stream interactions and shock identification that HAFv2 uses (which is the major difference between the models) does not adequately simulate the real situation or the error in arrival times resides in an aspect of the modeling that the three models share. This aspect may be the blast-wave formulation, which has been abandoned by many in the modeling community in favor of CME-driven shocks (see below).

Of greater concern to the forecaster than the difference between 12-h and 14-h errors in predicted arrival times are false alarms and false all-clears. Here model performance shows room for significant improvement. In all three cases, about 50% of predicted shocks do not arrive within one day of the predicted time, and after about 25% of predicted no-shocks, shocks arrive anyway.

False alarms statistics are more favorable for predictions based on halo CME signatures as used in the empirical algorithms. From a catalog of 328 entries documenting either CMEs or ICME signatures (including shocks), Schwenn *et al*. (2005) found that 85% of front-side halo CMEs were followed by an ICME disturbance at Earth. The remaining 15% of ICMEs evidently missed the Earth, which perhaps represents an irreducible false alarm rate for predictions based on halo CMEs alone.

Significant reductions in the error of predicted arrival times and of false alarms will probably not happen until full-up numerical codes become operational that self-consistently integrate the equations of motion of the entire Sun-to-Earth medium – the corona, the solar wind, the CME and the ICME. As discussed in Section 3.2 of Forbes *et al*. (2006, this volume), such codes are being constructed and tested but are still in the development stage. Readers interested in what the future offers in this area can consult reports on two ambitious space-weather-code-development projects: the Center for Integrated Space Weather Modeling (CISM) (Hughes and Hudson, 2004) and the Space Weather Modeling Framework (SWMF) (Tóth *et al*., 2005).

3. Intensities of CME Disturbances

3.1. Geoeffective Solar Wind Parameters

Solar wind parameters most effective in causing magnetospheric storms are speed, southward-pointing magnetic field, and dynamic pressure (ρV^2) (e.g., Srivastava and Venkatakrishnan, 2004). The speed and magnetic field work in combination to generate the geoeffective component of the interplanetary electric field

($IEF = -\mathbf{V} \times \mathbf{B}$). Thus, more concisely, the geoeffective parameters are the geoeffective component of the *IEF* and ram pressure; but, as a practical matter, the speed, magnetic field, and density that make up the *IEF* and the ram pressure are separate forecast operations. (In the following, whenever the interplanetary magnetic field (IMF) is mentioned in the context of geoeffectiveness, the radial-from-the-Sun component is regarded to be zero, since it has little effect on storm intensity, and it complicates the discussion to retain it.)

The strength of the voltage across the polar cap, $\Phi_{\rm PC}$, (which drives ionospheric currents that produce high-latitude magnetic disturbances) is a convenient parameter to illustrate the separate roles that the *IEF* and the dynamic pressure, P_D, have in causing geomagnetic effects. This is because there is an analytic expression relating the three variables, which has the form (Siscoe *et al.*, 2002)

$$\Phi_{\rm PC} = \frac{C_1 P_D^{1/3} IEF g(\theta)}{P_D^{1/2} + C_2 IEF g(\theta)} \tag{4}$$

where C_1 and C_2 are constants determined by theory and $g(\theta)$ is the (highly difficult-to-predict, see below) 'coupling-strength function', which depends on the angle, θ, between the IMF and the geomagnetic dipole. $g(\theta)$ ranges from unity when $\theta = 0^\circ$ to zero when $\theta = 180^\circ$. Figure 4 shows a plot of contours of constant $\Phi_{\rm PC}$ in the $P_D - IEF$ plane assuming maximum coupling ($g(\theta) = 1$). For small *IEF*, $\Phi_{\rm PC}$ is nearly independent of P_D; whereas for large *IEF*, the dependence on P_D becomes substantial while the dependence on *IEF* weakens considerably (so called transpolar potential saturation).

In a CME-induced magnetospheric storm, the disturbance arrives in two stages. First comes the ICME sheath, the wave of disturbance that precedes an ICME if it is

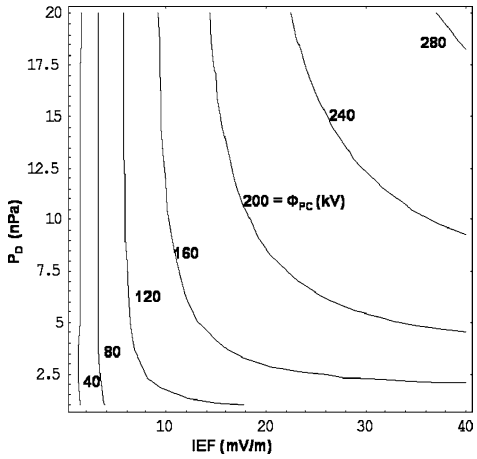

Figure 4. Contours of constant $\Phi_{\rm PC}$ in the $P_D - IEF$ plane illustrating the control of the solar wind parameters *IEF* and P_D on a geomagnetic disturbance parameter (from Siscoe *et al.*, 2002).

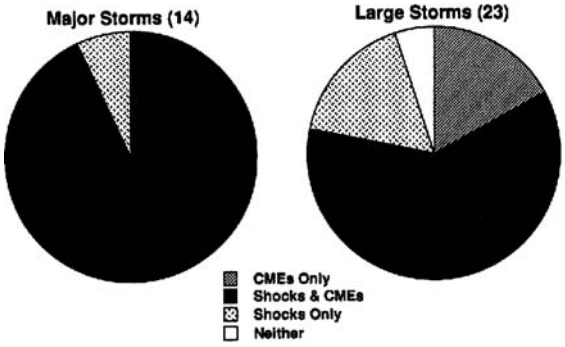

Figure 5. Pie charts showing relative occurrence frequency of 'Major Storms' (those with storm index *Kp* greater than 8-) and 'Large Storms' (*Kp* between 7- and 8-) that are caused by ICMEs without shocks, shocks without ICMEs, both together, and neither (from Gosling *et al.*, 1991).

plowing into the solar wind ahead of it, then the ICME itself, unless it is a glancing passage. As Figure 5 from Gosling *et al.* (1991) shows both the ICME sheath ('Shocks Only') and ICMEs by themselves ('CMEs only') can be geoeffective. But the one-two punch of an ICME-sheath followed by an ICME produces the most intense storms.

To illustrate what tools are currently available to predict storm intensity, it suffices to consider the ideal case in which solar indicators (halo CME, type II radio burst, X-ray duration and intensity, and the location of the associated flare or disappearing solar filament) tell the forecaster to expect a direct hit by a fast ICME and its shock. Then the forecaster considers the speed, magnetic field, and density in the ICME sheath and, separately, in the ICME body.

3.2. Geomagnetic Disturbances Induced by ICME Sheaths

Regarding the ICME sheath, Equation (5) gives an empirically-derived algorithm relating the maximum ICME-related solar wind speed, V_{Max}, at 1 AU to the shock transit time, T_{SH} (after Cliver *et al.*, 1990):

$$V_{\mathrm{Max}}(\mathrm{km/s}) = \frac{32,292}{T_{\mathrm{SH}}(\mathrm{h}) - 40} \tag{5}$$

Presumably this maximum speed is reached at the leading edge of the ICME and, thus, represents also the maximum speed in the ICME. The relevant point for forecasting is that T_{SH} can be predicted from the Schwenn *et al.* algorithm (Equation (1)). Thus, one critical, intensity-determining parameter has an implementable forecast algorithm, albeit with an uncertainty that compounds the uncertainties of Equations (1) (standard deviation of 14 h) and (5) (correlation coefficient of 0.72).

A second of the critical, intensity-determining parameters – the maximum magnetic field strength B_{Max} – also has an implementable algorithm (Owens *et al.*, 2005)

that relates B_{Max} to V_{Max} of Equation (5) and, therefore, also to V_{exp} of Equation (1), as follows:

$$B_{\mathrm{Max}}(\mathrm{nT}) = 0.047\, V_{\mathrm{Max}}(\mathrm{km/s}) + 0.06 \tag{6}$$

The uncertainty in applying Equation (6) to predict B_{Max} from V_{exp} now comprises the uncertainties in Equations (1), (5), and (6) (correlation coefficient of 0.83 (0.90 for the Owens *et al*. equation for the average sheath field strength)).

One expects the field to maximize also at the leading edge of the ICME (as for the magnetosheath at the nose of Earth's magnetosphere). Thus multiplying Equations (5) and (6) gives a prediction algorithm for the maximum value of the *IEF* in the CME sheath (but not necessarily a good prediction of the maximum geoeffective component of the *IEF* – see below). The uncertainty in this case is a fifth-order concatenation of composite uncertainties.

The third critical, intensity-determining parameter is density, n. Since post-shock flow is approximately incompressible, density could, in principle, be computed from the shock jump conditions and a prediction of the pre-shock solar wind conditions from solar data such as given by the Wang-Sheeley-Arge model (WSA) (Arge and Pizzo, 2000), where the ICME leading speed, V_{Max} would be used for the shock speed. In its present form, however, the WSA model predicts speed and IMF polarity but neither density nor magnetic field strength. Thus, one must use climatological values for these. Consequently, in a prediction algorithm for ICME-sheath density constructed from empirical formulas, the uncertainty would appear to be as great as those for V_{Max} and B_{Max}. Only in the case of a predicted fast ICME with a high-Mach-number shock would the uncertainty be reduced, for then the post-shock density is (to a good approximation) four times the pre-shock density, and the uncertainty is restricted to the uncertainty in determining the pre-shock density value. On the other hand, fast shocks are of greatest interest to the forecaster, so the situation is not as bad as it seems at first.

Regarding empirically-based algorithms for predicting the magnitudes of the intensity-determining parameters B, V, and n in an ICME sheath from near-Sun observations, one must conclude that there is a need to develop formulas that directly relate the desired quantities (B, V, and n or, better, the products BV and nV^2) to the observed solar quantities (as has been done for the shock arrival time, e.g., Equation (1)) to avoid the growth of uncertainties that results from concatenating forecast algorithms.

The physics-based forecast codes, STOA and ISPM, predict shock strength at Earth based on their estimates of initial energy in the disturbance. From the shock strength thus predicted, some estimate of ICME-sheath parameters can be computed from shock jump conditions, but again the pre-shock values needed for input to the computation must be provided by some extra-algorithmic procedure. And so, as in the empirical algorithms, there is a concatenation of uncertainties. The HAFv2 code does predict ICME-sheath parameters including B, V, and n. At present this is the most comprehensive code available for operational forecasts of geoeffective

ICME-sheath parameters; but, as of now, an assessment of its forecast skill has not been published.

The greatest uncertainty in forecasting the intensity of the disturbance that an ICME sheath will produce resides in predicting the coupling-strength function, $g(\theta)$ (Equation (4)), which multiplies the quantity usually taken to be the dominant measure of potential solar wind geoeffectiveness, the *IEF*. Although $g(\theta)$ varies from 1 when the IMF is south-pointing ($\theta = 0^\circ$) to 0 when the IMF is north-pointing ($\theta = 180^\circ$), its long-term average is about 0.25, based on the formula $\cos^4(\theta/2)$ that yields the greatest correlation coefficient between $VBg(\theta)$ and geomagnetic disturbance indices (Newell *et al*., 2006). This value, corresponding to $\theta \sim 90^\circ$, is reasonable because on a long-term average the IMF lies in the heliographic equatorial plane, approximately perpendicular to Earth's magnetic dipole.

The problem in predicting $g(\theta)$ in an ICME sheath is that the sheath is usually highly turbulent, and turbulence is inherently unpredictable. For example, McPherron and Siscoe (2004) estimated that the turbulence in the solar wind (not the turbulence in ICME sheaths, which is greater) causes the IMF to alternate randomly between northward tilting and southward tilting (relative to the heliographic equator) about 600 times between the Sun and Earth, or about every 10 minutes. An ICME sheath will compress and speed up the alternations so that the geomagnetic response,which takes typically 15 minutes or longer, acts like a low-pass filter to the IMF fluctuations. The statistical characteristics of IMF turbulence in ICME sheaths has yet to be studied using filters that simulate the magnetospheric response to the *IEF*. Such a project could lead to useful probabilistic forecasts of ICME-sheath disturbances (McPherron and Siscoe, 2004). The problem of forecasting the $g(\theta)$ caused by large-amplitude IMF turbulence in ICME sheaths is unlikely to be solved through deterministic (non-probabilistic) codes of any description.

Of greater importance to the forecaster are systematic southward or northward tilts of the IMF in ICME sheaths since these can bias $g(\theta)$ to high or low values, respectively. Systematic out-of-equatorial tilts can arise from shock deflection and field-line draping around the ICME body (Gosling and McComas, 1987; McComas *et al*, 1989; Wu and Dryer, 1996).

Figure 6 from McComas *et al*. (1989) illustrates their use as a forecast aid. It shows a CME launched from the northern solar hemisphere propagating into an IMF that points towards the Sun. The IMF tilts southward in the region of the ICME sheath that will reach Earth and thus be geoeffective. If the IMF pointed away from the Sun, it would tilt northward in the sheath and not be geoeffective. Extension to CMEs launched from the southern solar hemisphere is obvious. McComas *et al*. (1989) found that 13 of 17 events analyzed (77%) obeyed the draping prediction rule.

The most reliable predictor of a systematic bias in $g(\theta)$ comes from the variation of the tilt of the geomagnetic dipole relative to the ecliptic plane (which combines a 23.5° tilt of the rotation axis with a 11.5° tilt of the dipole relative to the rotation axis and, so, can be as great as 35°). Through a consideration of the geometry of

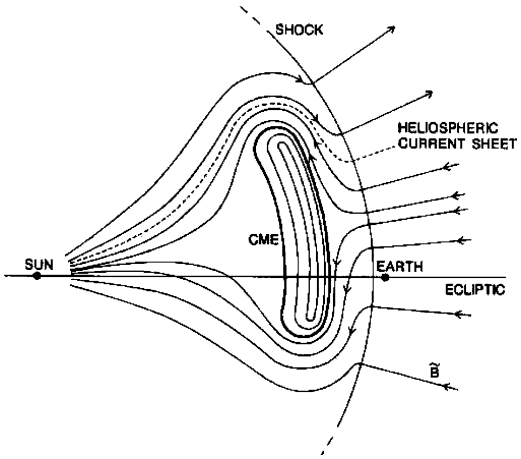

Figure 6. Out-of-equatorial tilting of the IMF cause by transiting of an off-equatorial ICME (from McComas *et al*., 1989).

the seasonal variation of the dipole tilt relative to the geoeffective component of a Parker-spiral IMF, Russell and McPherron (1973) showed that the tilt-bias in $g(\theta)$ should maximize around the equinoxes (which, by coincidence, is close to where Earth's orbit runs parallel to the heliographic equator, thus minimizing the complicating effect of the 7.25° tilt of the ecliptic relative to it). Then even for the idealized case in which the IMF has no tilt to the equatorial plane, the value of $g(\theta)$ systematically can be considerably greater than its average 0.25 value (more than 0.6 for favorable IMF coupling) or considerably less (under 0.1 for unfavorable IMF coupling). This so-called "Russell-McPherron effect" is predictable from solar observations by the previously-mentioned Wang-Sheeley-Arge model.

3.3. Geomagnetic Disturbances Induced by ICME Bodies

The previous section reduced the problem of forecasting geomagnetic disturbances to the problem of predicting the geoeffective parameters VB, $g(\theta)$ and nV^2 in ICME sheaths. This section looks at how well these parameters can be predicted for ICME bodies. Two preliminary remarks are in order. First, the phenomenology that these parameters display in ICME bodies is completely different than in ICME sheaths; thus, nothing in the previous section regarding phenomenology applies here. Second, "ICME bodies" is a non-unique description. It could mean a magnetic cloud, or a cloud-like structure (having the magnetic but not the thermal signature of a cloud), or a non-cloud-like structure (see Zurbuchen and Richardson, 2006, this volume). Unfortunately, which type actually materializes cannot be predicted from solar observations at present. Only for magnetic clouds and cloud-like structures have disturbance forecast algorithms based on solar observations been developed.

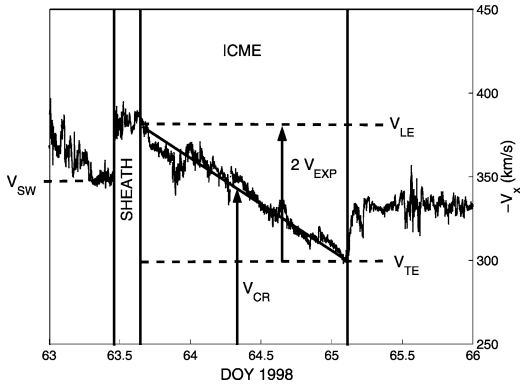

Figure 7. Velocity profile of a cloud or cloud-like ICME and the associated preceding and trailing flows. The figure defines the pre-event solar wind speed, V_{SW}, the leading-edge speed, V_{LE}, the cruise speed, V_{CR}, the trailing-edge speed, V_{TE}, and the expansion speed, V_{EXP} (from Owens *et al.*, 2005).

Estimates of the fraction of ICMEs that fall into the predictable, cloud-or-cloud-like category vary from 14% to 80% (depending on criteria used) with numbers less than 50% dominating, (Richardson and Cane, 2004). Consequently, even before a disturbance forecast algorithm based on solar observations for a cloud-or-cloud-like ICME is brought into play, an initial uncertainty of the order of 50% exists in whether such an algorithm in fact applies, and this existential reality must be incorporated in assigning a reliability tag to the forecast. (As discussed below, however, the situation improves dramatically for shorter range, yet still useful, forecasts.)

Consider then forecast procedures based on solar observations that apply to cloud and cloud-like ICMEs. As in the case of forecast procedures for ICME-sheath disturbances, procedures for ICME-body disturbances pertain to V, B, $g(\theta)$ and n separately (not to their geoeffective combinations), but with an important exception. Regarding n, there is as of yet no prediction procedure except for invoking climatology; for example, the profile of the average value of n through a magnetic cloud (based on a sample of 19 clouds) varies between 10 and 15 protons/cm^3 (Lepping *et al.*, 2003). The variation from this average profile is known to be large, however, especially toward interesting high values; but statistics from a large enough sample to define the extremes is lacking at present.

Forecast algorithms for ICME bodies based on solar observations exist for V, B and $g(\theta)$. Concerning first V, Owens *et al.* (2005) distinguish between the speed of the leading edge of an ICME, V_{LE}, and the 'cruise speed', V_{CR}, by which is meant the speed averaged over the time that the body passes. Figure 7 from the cited paper illustrates the definitions of the two speeds and defines also a 'trailing-edge speed', V_{TE}, and an ICME 'expansion speed', V_{EXP}, (not to be confused with the halo expansion speed discussed in Section 2.1). For the case of a linear velocity profile, as here, V_{CR} is simply the average of V_{LE} and V_{TE}.

The relevance of this work to forecasting is that Owens *et al.* (2005) give empirical relations for the rate at which the speed decreases within the ICME, m_{EXP}, in terms of V_{LE}, which is the same as V_{Max} of the previous section, for which Equation (5) allows predictions from solar observations:

$$m_{\mathrm{EXP}} = 10^{-8}\left(1.19\, V_{\mathrm{LE}}^2 - 954\, V_{\mathrm{LE}} + 284,180\right)\ \mathrm{km/s}^2 \tag{7}$$

with a correlation coefficient of 0.9. Thus, the velocity profile through the cloud, $V_{\mathrm{CME}}(t)$, is predictable from solar observations according to

$$V_{\mathrm{CME}}(t) = V_{\mathrm{LE}} - m_{\mathrm{EXP}}\, t \tag{8}$$

The ICME ends when $V_{\mathrm{CME}}(t)$ falls to $V_{\mathrm{TE}} = V_{\mathrm{LE}} - 2V_{\mathrm{EXP}}$, for which Owens *et al.* (2005) provide the empirical relation.

$$V_{\mathrm{EXP}}(\mathrm{km/s}) = 0.266\, V_{\mathrm{LE}} - 70.6\ \mathrm{km/s} \tag{9}$$

Equations (7)–(9) together with (5) constitute a complete forecast algorithm for the velocity within an ICME magnetic cloud. They can also be used to calculate the radial half-thickness of ICME clouds, which yields values between 0.15 AU and 0.2 AU across the observed range of ICME speeds.

The other disturbance-inducing ICME parameter that is (in principle) predictable from solar observations are B and $g(\theta)$. Regarding $g(\theta)$, the state of the art is such that instead of actually predicting $g(\theta)$, one is usually limited to making a binary prediction as to whether the IMF in the ICME cloud points in a direction that favors (southward) or disfavors (northward) strong coupling to the magnetosphere, that is, in effect, whether $g(\theta)$ is close to 1 or to 0.

The forecast procedure in this case is based on the geometry of magnetic flux ropes, which ICME magnetic clouds approximate (e.g., Forsyth *et al.*, Wimmer-Schweingruber *et al.*, Zurbuchen and Richardson, 2006, this volume). The magnetic field in a flux rope has an axial component and a toroidal component (see Figure 2 in Forsyth *et al.*, 2006, this volume). If the axis of the flux rope lies more perpendicular than parallel to the axis of the geomagnetic dipole, the toroidal component dominates in determining $g(\theta)$. In this case the magnetic field will be oriented favorably for coupling in half of the rope and unfavorably in the other half, but there will always be an interval of favorable coupling. The only issue is whether it comes in the leading or trailing half of the cloud. On the other hand, if the axis of the flux rope lies more parallel than perpendicular to the axis of the geomagnetic dipole, the flux rope's axial component dominates in determining $g(\theta)$. An either-or situation results: either the magnetic field in the flux rope is oriented favorably or unfavorably for strong coupling throughout the passage of the cloud over Earth. Faced with on oncoming ICME flux rope, the forecaster is therefore interested in predicting the angle between the flux rope's axis and the axis of the geomagnetic dipole (greater than or less than 45°) and the directions of its axial and toroidal magnetic field components.

An example in which such a forecast procedure has been tested is described by Zhao and Hoeksema (1997). They define the latitude of the flux rope axis to be the angle between it and the ecliptic plane with positive latitudes corresponding to a northward axial magnetic field component. Then latitudes between $+/-45^\circ$ correspond to flux ropes more perpendicular to the dipole axis (they ignored the tilt of the dipole relative to the ecliptic), and latitudes poleward of $+/-45^\circ$ correspond to flux ropes more parallel to the dipole axis. Using data from 23 magnetic flux ropes, they plotted the duration of strong-coupling intervals against cloud-axis latitude. They obtained the expected result, that the duration varies systematically (albeit with appreciable scatter) from close to zero for a latitude of $+90^\circ$ to a maximum value for -90°, corresponding to a $\sim$20-h transit through favorable fields in the entire flux rope. Similarly, they found that the intensity of the geoeffective component of the magnetic field in the clouds also varied systematically with axis latitude in the expected sense from essentially zero to about 20 nT.

The linear fits to the Zhao and Hoeksema data provide the first step needed for a forecast algorithm:

$$D(\mathrm{h}) = (11.49 - 0.12\,L_E) \pm 4.70 \tag{10}$$

$$Bg(\theta)\,(\mathrm{nT}) = (10.76 - 0.10\,L_E) \pm 5.12 \tag{11}$$

where D is duration in hours, $Bg(\theta)$ is the geoeffective intensity in nT (this is the negative of the Zhao and Hoeksema intensity, I, which is modeled after the northward rather than the geoeffective southward component of the IMF), and L_E is the ecliptic latitude (in degrees) of the flux rope axis. Zhao and Hoeksema complete the task of developing a forecast algorithm by relating L_E to a solar observable associated with the release of the CME, a disappearing solar filament, DSF, following the findings of Bothmer and Rust (1997) and Bothmer and Schwenn (1998) that the orientation of magnetic clouds is well-correlated with the orientation of the source filament on the Sun (see also the discussion in Forsyth *et al.*, 2006, this volume). A DSF has a defined axis, the orientation of which relative to the solar equator measured in degrees, *Fo*, determines L_E according to the empirical formula

$$L_E(\mathrm{deg}) = (-1.4 + 0.7Fo) \pm 17.8 \tag{12}$$

Equations (10)–(12) make up a forecast algorithm $Bg(\theta)$ for inside cloud and cloud-like ICMEs. It is, of course, important to carry out a test of the response of the magnetosphere to the $V\,Bg(\theta)$ predicted by Equations (5) and (7)–(12).

3.4. Intermediate-Term Forecasts With L1 Data

Forecasts based on solar observations at the time of the release of the CME offer a one- to four-day advance warning of the oncoming disturbance. Nowcasts based on L1 observations that merely note what is arriving as it arrives give less than

one-hour advance warning. There is an intermediate forecast range that uses L1 data together with models to predict what is yet to arrive from what has already arrived. Since a CME disturbance can last more than 24 hours, there is room for useful forecasts in the 10-hour range from L1 observations.

Chen *et al*. (1997) first noted the possibility of making intermediate range forecasts with real-time L1 observations. For example, such observations quickly eliminate the uncertainty (of the order of 50%) regarding whether or not the ICME body is a magnetic cloud (or cloud-like). Chen *et al*. developed a pattern-recognition program that can identify a magnetic flux rope and its orientation after sampling about 20% of it. The remaining 80%, therefore, becomes predictable by fitting to analytical models whose parameters have been determined with data from archived events. The technique already shows successful results and has the capability for improvements by incorporating more aspects of cloud dynamics.

A second forecast procedure of this type has been proposed by Owens *et al*. (2005), in their case based on Equations (7)–(9). Instead of using Equation (5) to determine the leading-edge speed, V_{LE}, from solar observations (and, so, several days in advance), one can measure it when the ICME reaches L1. Then one can instantly calculate from the equations the velocity profile through the ICME and the duration of its passing over Earth. They also note that once the shock arrives, its speed can be calculated instantly from the shock jump relations. Since the shock speed should be the same as the speed of the leading edge of the ICME, which is V_{Max} in Equation (6), from that equation one can then determine B_{Max} in the sheath several hours before the maximum field arrives. Continuing in the same vein, one can use the Chen *et al*. procedure to determine L_E in Equations (10) and (11), to update the forecast obtained from Equation (12). It appears that the possibilities for exploiting intermediate range forecasting with L1 observations are considerable.

4. Summary

Algorithms to predict the arrival time of a CME disturbance (its shock or the ICME itself) from solar observations exist in both empirical, data-based versions and physics-based versions. The empirical algorithms have errors at the 95% confidence level of about 1 day. Physics-based algorithms do a little better but forecast significantly more false alarms. Inhomogeneities in the solar wind through which the shock travels before reaching Earth impose an irreducible uncertainty of the order of 10 hours on any algorithm that does not take them into account. The best hope for improvement in this area is through numerical integrations of the operative equations of motion that self-consistently incorporates the corona, the CME, and the solar wind.

Algorithms that use solar observations to forecast the geoeffective solar wind parameters (VB, $g(\theta)$ and nV^2) in ICME sheaths can be concatenated out of existing formulas that have been developed for other purposes. But the growth of uncertainty

that concatenating algorithms entails might reduce their skill relative to climatology essentially to zero or less – the evaluation has not been performed. It would be good to develop and evaluate algorithms that forecast geoeffective quantities directly from solar observations. The problem that strong IMF turbulence in ICME sheaths imposes on forecasting is probably irreducible and will have to be addressed through probabilistic forecast protocols. Nonetheless, under rare conditions with a high potential for a space-weather impact – a super-fast, Earth-directed, Sun-centered halo CME during equinox with a WSA prediction of maximum $g(\theta)$ from the Russell-McPherron effect – a forecast of a strong ICME-sheath disturbance might be made with reasonable confidence. This is a best-case scenario.

Algorithms that use solar observations to forecast the geoeffective solar wind parameters in ICME bodies are beset from the start with an uncertainty (on the order of 50%) whether a forecasted ICME arrival at Earth will bring a predictable-in-principle magnetic cloud ICME or a so-far unpredictable non-cloud ICME. If a cloud ICME arrives, data-based algorithms exist to predict many of its parameters from the time of the CME initiation: the velocity profile through the ICME and the geoeffective component of the magnetic field. These algorithms, however, are based on a prediction algorithm for the speed of the leading edge of the ICME in one case and on the angle that the ICME axis (viewed as a flux rope) makes to the ecliptic plane in the other case. Thus there is also a growth of uncertainties owing to a concatenation of algorithms.

Uncertainty over which type of ICME will materialize and growth of uncertainty owing to concatenations of algorithms can be dramatically reduced by using L1 data to specify crucial input parameters to the forecast codes. The price is a loss in forecast range from more than one day to less than one day.

Acknowledgements

This work was supported in part by the US National Science Foundation under grant ATM-0220396 and by the CISM project which is funded by the STC Program of the National Science Foundation under Agreement Number ATM-0120950.

References

Arge, C. N., and Pizzo, V. J.: 2000, *JGR* **105**, 10,465.

Bothmer, V., and Rust, D. M.: 1997, in: Crooker, N.U., Joselyn, J.A., and Feynman, J. (eds.), *Coronal Mass Ejections*, *Geophys. Monogr. Ser.*, vol. 99, AGU, Washington, D.C., pp. 137–146.

Bothmer, V., and Schwenn, R.: 1998, *Ann. Geophys.* **16**, 1–24.

Cane, H. V., and Richardson, I. G.: 2003, *JGR* **108**, A41156, doi:10.1029/2002JA009817.

Carlowicz, M. J., and Lopez, R. E.: 2002, *Storms from the Sun*, The Joseph Henry Press, Washington, DC.

Chen, J., Cargill, P. J., and Palmadesso, P. J.: 1997, *JGR* **102**, 14,701.

Cliver, E. W., Feynman, J., and Garrett, H. B.: 1990, *JGR* **95**, 17103–17112.

Crooker, N. U.: 2000, *JASTP* **62**, 1071–1085.

Dal Lago, A., Schwenn, R., and Gonzalez, W. D.: 2003, *Adv. Space Res.* **32**, 2637–2640.
Dryer, M.: 1974, *Space Sci. Rev.* **15**, 403–468.
Echer, E., Gonzalez, W. D., and Alves, M. V.: 2006, *Space Weather* **4**, S06001, doi:10.1029/2005SW000200.
Forbes, T. G., Linker, J. A., *et al.*: 2006, *Space Sci Rev.*, this volume, doi: 10.1007/s11214-006-9019-8.
Forsyth, R. J., Bothmer, V., *et al.*: 2006, *Space Sci. Rev.*, this volume, doi: 10.1007/s11214-006-9022-0.
Freeman, J. W.: 2001, *Storms in Space*, Cambridge University Press, Cambridge.
Fry, C. D., Sun, W., Deehr, C. S., Dryer, M., Smith, Z., Akasofu, S.-I., *et al.*: 2001, *JGR* **106**, 20,985–21,001.
Fry, C. D., Dryer, M., Smith, Z., Sun, W., Deehr, C. S., and Akasofu, S.-I.: 2003, *JGR* **108**, A21070, doi:10.1029/2002JA009474.
Gopalswamy, N., Lara, A., Lepping, R. P., Kaiser, M. L., Berdichevsky, D., and O. C. St. Cyr.: 2000, *GRL* **27**(2), 145–148.
Gopalswamy, N., Lara, A., Yashiro, S., Kaiser, M. L., and Howard, R. A.: 2001, *JGR* **106**, A12, 29,207–29,217.
Gosling, J. T., and McComas, D. J.: 1987, *GRL* **14**, 355–358.
Gosling, J. T., McComas, D. J., Phillips, J. L., and Bame, S. J.: 1991, *JGR* **96**, 7831–7839.
Heinemann, M.: 2002, *JASTP* **64**, 315–325.
Hughes, W. J., and Hudson, M. K.: 2004, *JASTP* **64**, 1241–1242.
Joselyn, J. A.: 1995, *Rev. Geophys.* **33**(3), 383–401.
Lepping, R. P., Berdichevsky, D. B., Szabo, A., Arqueros, C., and Lazarus, A. J.: 2003, *Solar Physics* **212**, 425–444.
McComas, D. J., Gosling, J. T., Bame, S. J., Smith, E. J., and Cane, H. V.: 1989, *JGR* **94**, 1465–1471.
McPherron, R. L., and Siscoe, G.: 2004, *Space Weather* **2**, S01001, doi:10.1029/2003SW000003.
Newell, P. T., Soterelis, T., Liou, K., Meng, C., and Rich, F. J.: 2006, *Eos Trans. AGU* **87**(36), Jt. Assem. Suppl., Abstract SM41D-04.
Odenwald, S.: 2001, *The 23rd Cycle*, Columbia University Press New York.
Owens, M. J., Cargill, P. J., Pagel, C., Siscoe, G. L., and Crooker, N. U.: 2005, *JGR* **110**, A01105, doi:10.1029/2004JA010814.
Parker, E. N.: 1963, *Interplanetary Dynamical Processes*, Interscience Publishers.
Richardson, I. G., and Cane, H. V.: 2004, *GRL* **31**, L18804, doi:10.1029/2004GL020958.
Russell, C. T., and McPherron, R. L.: 1973, *JGR* **78**, 92–108.
Russell, C. T., and Mulligan, T.: 2002, *Planet. Space Sci.* **50**, 527.
Schwenn, R., Dal Lago, A. Gonzalez, W. D. Huttunen, E. Cyr, C. 0. St., and S. Plunkett P.: 2001, *Eos Trans. AGU* **82**, 47, Fall Meet. Suppl., Abstract SH12A-0739.
Schwenn, R., Dal Lago, A., Huttunen, E., and Gonzalez, W. D.: 2005, *Ann. Geophys.* **23**, 1033–1059.
Schwenn, R.: 2006, *Living Rev. Solar Phys.* **3**, 2. URL (cited on July 10, 2006): http://www.livingreviews.org/lrsp-2006-2.
Siscoe, G. L., Erickson, G. M., Sonnerup, B. U. Ö., Maynard, N. C., Schoendorf, J. A., Siebert, K. D., *et al.*: 2002, *J. Geophys. Res.* **107**(A6), 1075, doi10.1029/2001JA000109.
Smith, Z., and Dryer, M.: 1990, *Sol. Phys.* **129**, 387–405.
Smith, Z., Dryer, M., Ort, E., and Murtagh, W.: 2000, *JASTP* **62**, 1265–1274.
Srivastava, N., and Venkatakrishnan, P.: 2004, *JGR* **109**, A10103, doi:10.1029/2003JA010175.
Tóth, G., *et al.*: 2005, *JGR* **110**, A12226, doi:10.1029/2005JA011126.
Wimmer-Schweingruber, R. F., Crooker, N. U., et al.: 2006, *Space Science Reviews*, this volume, doi: 10.1007/s11214-006-9017-x.
Wu, C. C., and Dryer, M.: 1996, *JGR* **23**, 1709–1712.
Zhao, X. P., and Hoeksema, J. T.: 1997, *GRL* **24**(23), 2965–2968.
Zurbuchen, T. H., and Richardson, I. G.: 2006, *Space Science Reviews*, this volume, doi: 10.1007/s11214-006-9010-4.